In-situ growth and immobilization of CdS nanoparticles onto functionalized MoS_2: preparation, characterization and fabrication of photoelectrochemical cell

Antonia Kagkoura, Javier Hernández-Ferrer, Ana M. Benito, Wolfgang K. Maser, Nikos Tagmatarchis

CHEMISTRY AN ASIAN JOURNAL

which has been published in final form at https://doi.org/10.1002/asia.201901371 on 26th of November 2019.

In-situ growth and immobilization of CdS nanoparticles onto functionalized MoS_2: preparation, characterization and fabrication of photoelectrochemical cell

Antonia Kagkoura,[a] Javier Hernandez-Ferrer,[b] Ana M. Benito,[b] Wolfgang K. Maser[b], Nikos Tagmatarchis*[a]

Abstract: A facile strategy for the controllable growth of CdS nanoparticles at the periphery of MoS_2 en route the preparation of electron donor-acceptor nanoensembles is developed. Precisely, the carboxylic group of α-lipoic acid, as addend of the modified MoS_2 obtained upon 1,2-dithiolane functionalization, was employed as anchor site for the in-situ preparation and immobilization of the CdS nanoparticles in an one-pot two-step process. The newly prepared MoS_2/CdS hybrid material was characterized by complementary spectroscopic, thermal and microscopy imaging means. Absorption spectroscopy was employed to register the formation of MoS_2/CdS, by observing a broad shoulder centered at 420 nm due to CdS nanoparticles, while the excitonic bands of MoS_2 were also evident. Moreover, based on the efficient quenching of the characteristic fluorescence emission of CdS at 725 nm by the presence of MoS_2, strong electronic interactions at the excited state between the two species within the ensemble were identified. Photoelectrochemical assays of MoS_2/CdS thin-film electrodes revealed a prompt, steady and reproducible anodic photoresponse during repeated on-off cycles of illumination. A significant zero-current photopotential of -540 mV and an anodic photocurrent of 1 μA were observed, underlining improved charge-separation and electron transport from CdS to MoS_2. The superior performance of the charge-transfer processes in MoS_2/CdS is of direct interest for the fabrication of photoelectrochemical and optoelectronic devices.

Introduction

The increasing energy demand in modern society has roused exhaustive research to develop sustainable and renewable energy sources in order to reduce or completely replace fossil fuels. In solar energy conversion schemes, a plethora of versatile electron donors and acceptors are combined to yield functional hybrid materials that manage photoinduced charge-transfer processes. Particularly, in the last couple of decades, the field has been dominated by research with carbon nanostructures, giving rise to the development of numerous nanocarbon-based donor-acceptor systems with interesting photophysical and photoelectrochemical properties.[1-3] Conversely, although the structure and properties of transition metal dichalcogenides (TMDs) are nowadays well-studied,[4-6] little advances have been made towards hybridization with photo- and/or electro-active species and fabrication of electrodes for photoelectrochemical cells.

Exfoliated semiconducting MoS_2 nanosheets, one of the most studied TMDs, is considered as promising material in optoelectronics,[1] electrocatalysis[6-8] and energy-related applications.[3, 9] However, in order to fully profit from the exceptional properties of MoS_2, combination with other functional materials en route the development of advanced hybrids is a necessity. To this end, incorporation of organic units on TMDs can take place via covalent bonding or by supramolecular means.[10-12] In a recent methodology to functionalize TMDs and tune the optoelectronic properties, exfoliated semiconducting MoS_2 were functionalized with 1,2-dithiolanes at vacant sulfur sites located at the edges of the nanosheets.[13] Moving one step beyond, by employing 1,2-dithiolanes featuring a zinc phthalocyanine, the corresponding functionalization of MoS_2 resulted on the realization of a donor-acceptor hybrid material, in which bidirectional electron-transfer leading to a charge-separated state was observed.[14] Similarly, carbon dots and a porphyrin moiety have been integrated at the edges of exfoliated TMDs and allowed the development of photophysical events to take place.[15-18]

On the other hand, semiconducting quantum dots have been extensively used in light harvesting systems, due to their size dependent physicochemical properties.[19] Particularly, the ability to tune the absorption and emission of light of quantum dots according to their size and shape, makes them ideal candidates for energy conversion processes.[20, 21] Cadmium sulfide with a direct band gap of 2.4 eV, can absorb light effectively and is one of the most examined semiconductors for light harvesting applications. In addition, CdS nanoparticles are extremely stable and easy to fabricate. However, problems such as fast recombination of excitons can limit the full potential of CdS. To overcome this hurdle, nanocarbon-based materials were employed as support for CdS and diverse strategies applied to fabricate electron donor-acceptor type hybrids,[9] in condensed media and/or as integrative components at electrode surfaces.[22] Moreover, recently, not only CdS but also other semiconducting nanoparticles were combined with MoS_2 forming heterostructures with intriguing optical as well as photo- and/or electro-catalytic properties.[23-26]

Development of novel synthetic approaches that involve easy and straightforward steps for the fabrication of MoS_2/CdS ensembles is of paramount importance. For p-n heterojunctions, MoS_2 is a perfect p-type material due to its narrow band gap, excellent thermal stability and electrostatic performance. Moreover, the realization of heterostructured ensembles of p- and n-type components results in the accumulation of photoexcited electrons in the coupling interface of the n-type side, and holes in the p-type component. This enables the separation of the photoinduced electrons and holes across the heterointerface, which favors the

[a] Dr. Antonia Kagkoura, Dr. Nikos Tagmatarchis*
Theoretical and Physical Chemistry Institute
National Hellenic Research Foundation
48 Vassileos Constantinou Avenue, Athens 11635, Greece
E-mail: tagmatar@eie.gr

[b] Dr. Javier Hernandez-Ferrer, Dr. Ana M. Benito, Dr. Wolfgang K. Maser
Instituto de Carboquimica, (ICB-CSIC)
C/Miguel Luesma Castan 4, E-50018, Zaragoza, Spain

Supporting information for this article is given via a link at the end of the document.

transportation and suppresses their recombination, which are both essential for efficient solar-energy conversion. In this context, CdS was loaded on MoS_2 by calcination and the heterojunction was tested against photocatalytic H_2 production.[26, 27] The MoS_2/CdS ensemble exhibited improved charge separation, hence, better photocatalytic activity than CdS alone, while MoS_2 could be used to replace noble metals in catalytic systems. In another approach, MoS_2/CdS heterostructure was developed by electrodeposition and chemical bath deposition that showed much higher visible-light photoelectrocatalytic activity and higher stability toward water splitting compared to pure CdS film.[23] To this end, MoS_2/CdS heterojunction solar cells, synthesized by an approach involving the growth of MoS_2 films with chemical vapor deposition on CdS films, revealed promising photovoltaic behavior.[28] However, most of the abovementioned synthetic routes involve complex procedures that require complicated steps involving high temperatures and materials with not very well defined structures.

In this work, exfoliated semiconducting MoS_2 sheets were initially functionalized with α-lipoic acid to specifically introduce carboxylic units at the periphery of the nanosheets (*f*-MoS_2). Afterwards, *f*-MoS_2 was employed as template for the in-situ synthesis and immobilization of CdS nanoparticles, similar with our previous strategy involving carbon nanotube/amphiphilic block copolymer nanoensembles.[29] Herein, the realization of MoS_2/CdS is reported, while ample light is shed on the photoelectrochemical properties of the ensemble. The newly formed MoS_2/CdS was complementary characterized by electron microscopy (TEM) imaging, spectroscopic (IR, Raman, EDX) and thermogravimetric analysis (TGA) means. In addition, the quantitative quenching of the characteristic emission of CdS by MoS_2 under visible-light irradiation revealed strong intra-ensemble electronic communication between the two species. Alongside, photoelectrochemical assays on electrodes, fabricated by depositing thin-films of MoS_2/CdS, further confirmed the establishment of charge-transfer processes, whereby electrons transferred from photoexcited CdS to MoS_2 led to an enhancement of photoanodic current generation accompanied by a substantial negative photopotential. The latter demonstrates the occurrence of efficient charge-separation within the MoS_2/CdS ensemble, in line with recent studies in which a water-soluble polythiophene as photoinduced electron donor was electrostatically coupled with TMDs for managing the performance of photoelectrochemical and optoelectronic processes.[30]

Results and Discussion

The formation of CdS semiconducting nanoparticles on *f*-MoS_2 was accomplished according to Scheme 1. The 1,2-dithiolane functionalization of exfoliated MoS_2 with α-lipoic acid occurred at edge defective sites, giving rise to the decoration of the periphery of the two-dimensional nanosheets with –COOH units.[15] The latter in *f*-MoS_2 were employed as a scaffold for the growth and immobilization of CdS nanoparticles. The growth and immobilization of CdS nanoparticles was realized following a two-step one-pot reaction protocol. Briefly, in the first step, the electrostatic association of cadmium cations was exchanged between cadmium acetate and the carboxylic acid species grafted onto *f*-MoS_2, yielding Cd^{2+} ions in the periphery of *f*-MoS_2. Subsequently, in the second step, thioacetamide was added to transform Cd^{2+} into CdS nanoparticles – upon addition of thioacetamide and mild thermal treatment, decomposition of the latter and in-situ generation of sulfur occurred, yielding CdS nanoparticles at sites where the cadmium cations were initially located in *f*-MoS_2. For performing blank/reference measurements, CdS in the absence of MoS_2 were similarly synthesized, by employing α-lipoic acid and cadmium acetate followed by thioacetamide.

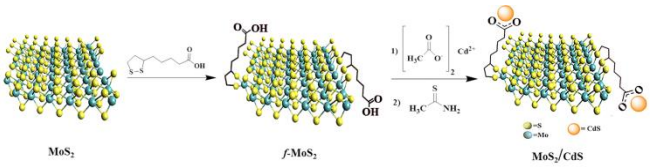

Scheme 1. Schematic representation of the fuctionalization of MoS_2 with α-lipoic acid and the subsequent preparation of the MoS_2/CdS ensemble.

The MoS_2/CdS ensemble was complementary characterized by microscopy imaging and spectroscopic techniques. TEM images of MoS_2/CdS clearly indicate round-shaped nanosized species with an average diameter of 1-2 nm, spread all over the MoS_2 nanosheets (Figure 1, left panel). EDX spectroscopy confirmed the presence of Cd, S and Mo elements, proving existence of CdS on MoS_2 sheets, together with that of C and O due to the organic addend on functionalized *f*-MoS_2 (Figure 1, right panel).

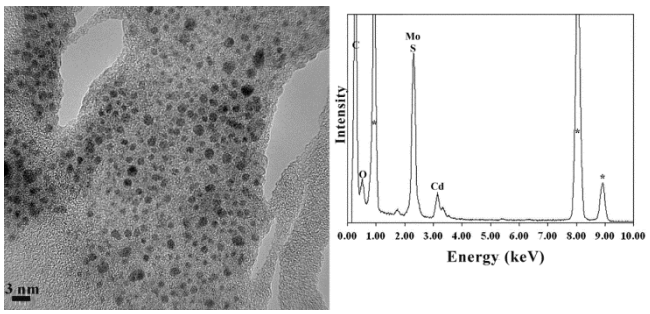

Figure 1. TEM image (left panel), and EDX spectrum of MoS_2/CdS ensemble (right panel). The Cu element, which is detected due to its presence in the sample holder, is denoted by *.

ATR-IR spectroscopy was employed to assess the functionalization of MoS_2 with lipoic acid and the formation of the MoS_2/CdS material. The IR spectrum of exfoliated MoS_2 is not rich in features. However, in the ATR-IR spectrum of *f*-MoS_2, a discrete band at 1720 cm^{-1} owed to –COOH units present in the addend was evident (Figure 2a). In addition, C-H stretching vibration bands owed to alkyl C-H on *f*-MoS_2 in the region 2800-3000 cm^{-1} verified the success of the functionalization. No further significant bands were identified in the IR spectrum of the MoS_2/CdS ensemble.

Raman spectroscopy (Figure 2b) was performed under on-resonance excitation conditions for MoS_2 (633 nm). Four dominant Raman active modes, namely, A_{1g}-LA(M), E^1_{2g}, A_{1g} and 2LA(M) at 177, 378, 405 and 450 cm^{-1}, respectively, were observed in the spectra of exfoliated MoS_2, *f*-MoS_2 and MoS_2/CdS. Particularly, the suppression of the 2LA(M) band in the Raman spectrum of *f*-MoS_2, directly related to sulfur vacancies, as compared to the one due to exfoliated MoS_2, proved the effective functionalization of MoS_2.[15] Furthermore, phonon modes related to the metallic polytype of MoS_2 were absent (i.e. typical J_1, J_2 and J_3 modes at 150, 225, and 325 cm^{-1}), confirming the semiconducting nature of MoS_2.[32]

Thermogravimetric analysis was performed to evaluate the loading of α-lipoic acid, and by extension of CdS nanoparticles, on MoS_2 (Figure 2c). Exfoliated MoS_2 is thermally stable under inert atmosphere up to 800 °C, while the mass loss observed beyond that temperature is ascribed to the decomposition of the lattice occurring at defected sites. In contrast, *f*-MoS_2 showed a mass loss of around 3 % in the temperature range 250-550 °C under nitrogen atmosphere due to the decomposition of the organic addend species. From the latter mass loss, the loading of organic addends was calculated to be 1 per every 40 MoS_2 units. Then, considering that CdS nanoparticles are formed and immobilized on the carboxylate units of *f*-MoS_2, the highest loading of CdS can be 1 per every 40 MoS_2 units.

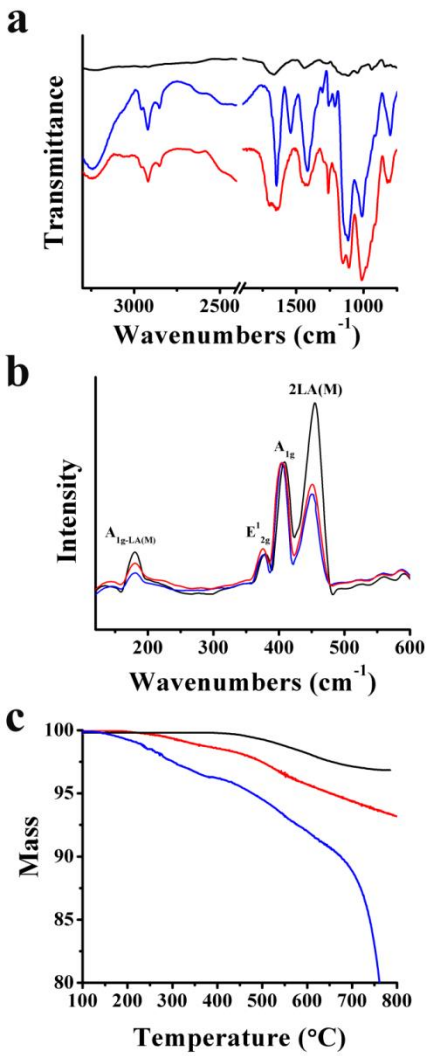

Figure 2. (a) ATR-IR spectra, (b) Raman spectra, and (c) TGA graphs for MoS_2 (black), *f*-MoS_2 (red) and MoS_2/CdS (blue).

Steady-state electronic absorption spectroscopy was employed to record the formation of the MoS_2/CdS ensemble (Figure 3a). In the absorption spectrum of MoS_2/CdS, a broad shoulder centered at 420 nm was evident, which is also present at the UV-Vis spectrum of bare CdS nanoparticles, employed as reference. Markedly, the absorption band of CdS is appreciably blue-shifted by 100 nm as compared to the one of macrocrystalline CdS and rationalized by considering the size quantization effects.[33] In addition, the excitonic bands of MoS_2 at 629 and 687 nm were also evident in the corresponding spectrum of the hybrid material. However, the broad absorption band due to CdS muffles the direct transitions from the valence band to the conduction band of MoS_2 in the region 400-500 nm.

Next, focusing on the electronic interaction interplay at the excited state, photoluminescence spectroscopic studies were carried out. The fluorescence emission spectrum of bare CdS nanoparticles (i.e. those without MoS_2 but stabilized by lipoic acid) was dictated by a broad band centered at 720 nm upon excitation at 420 nm. Notably, the characteristic emission of CdS in the MoS_2/CdS

ensemble was found highly quenched and also red-shifted at 725 nm. The suppression of photoluminescence for CdS is attributed to their effective immobilization of onto *f*-MoS_2, whereas also reveals the development of strong electronic interactions at the excited state between the two species. The latter is indicative of an alternative pathway for the transduction of energy from the excited state, involving energy/charge-transfer from photoexcited CdS to MoS_2 within the MoS_2/CdS ensemble.

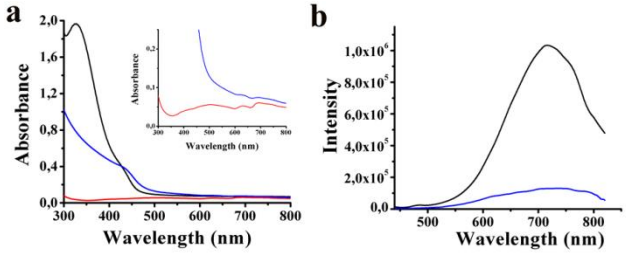

Figure 3. (a) UV-Vis absorption spectra for CdS (black), *f*-MoS_2 (red) and MoS_2/CdS (blue), obtained in DMF. Inset: expanded area of the absorption spectra for *f*-MoS_2 (red) and MoS_2/CdS (blue). (b) Photoluminescence spectra of CdS (black) and MoS_2/CdS (blue), obtained upon excitation at 420 nm in DMF.

Thin films of MoS_2/CdS were fabricated onto a fluorine-doped tin oxide electrode (FTO) via spray-coating and evaluated as photoanodes in photoelectrochemical cells. For reference purposes, thin films of *f*-MoS_2 as well as CdS were analogously spray-coated onto the electrode surface forming FTO/*f*-MoS_2 and FTO/CdS, respectively, and examined. The MoS_2 absorption features, appearing at 690, 630 and 504 nm dominated the electronic absorption spectrum of the FTO/MoS_2/CdS electrode, while the CdS absorption was centred at around 410 nm (Supporting Information, Figure S1). Furthermore, a background absorption that does not appear in the solution measurements was evident and assigned to scattering phenomena due to the film structure. This background was enhanced in the case of the FTO/MoS_2/CdS electrode. Considering that the films were of comparable thickness (please note that the same amount of material was sprayed onto the FTO substrate) the latter observation indicates a higher density of states at the Fermi level, most likely caused by interactions between MoS_2 and CdS. This leads to the development of effective intra-hybrid charge-transfer processes in the FTO/MoS_2/CdS electrode, and/or doping phenomena similar to those observed for carbon nanomaterials or TiO_2.[34-35] Conversely, the FTO/*f*-MoS_2 and FTO/CdS electrodes showed the excitonic absorption and semiconducting features of MoS_2 and CdS, respectively, in the visible region, mirroring the observations registered in solution (*cf*. Figure 3a). Next, photoelectrochemical measurements were conducted in a three-compartment cell, in acetonitrile containing 0.1 M $NaClO_4$ as redox electrolyte and the FTO/MoS_2/CdS as working electrode, while a graphite rod was employed as counter electrode. In dark voltammograms (Supporting Information, Figure S2), FTO/*f*-MoS_2 and FTO/CdS electrodes showed a typical capacitive response, with FTO/CdS including a minor resistive component. As for FTO/MoS_2/CdS, the dark voltammogram was similar to that of FTO/*f*-MoS_2 at potentials higher than -0.4 V. However, a cathodic current, which does not appear in the reference electrodes, was clearly observed, indicating that the combination and interactions of MoS_2 and CdS bring new electrochemical properties in MoS_2/CdS, which are not present in the individual components. Cyclic voltammetry assays under illumination revealed that the FTO/CdS electrode yields a photocathodic behavior (Figure 4a), typical of p-type electron donors,[36] where photoholes migrate to the electrode and photoelectrons are transferred to the solution. This photocathodic behavior is better observed in the on-off voltamogram (shown as inset at Figure 4a). On the other hand, FTO/*f*-MoS_2 exhibited an almost negligible photocurrent, with the corresponding on-off voltamogram showing an undefined non-stationary response with spikes (Supporting Information, Figure S3). In contrast to the individually examined materials, FTO/MoS_2/CdS showed a clear photoanodic behavior (Figure 4a), indicating a strong interaction and an effective charge-separation between MoS_2 and CdS. The latter performance is due to the development of photo-induced charge-transfer phenomena taking place at the excited state between CdS and MoS_2, with the former acting as electron donor and the latter as acceptor (*cf*. Figure 3b). This behavior is the same as that observed in quantum dot sensitized solar cells,[37] where quantum dots act as active materials, donating photoelectrons to TiO_2 or ZnO, which are not photoactive in the visible region. The different behavior of FTO/MoS_2/CdS as compared to the FTO/MoS_2 and FTO/CdS electrodes was confirmed by registering potentiostatic photocurrent transients at -0.5 and 0.8 V. The photocurrent response of the FTO/MoS_2/CdS electrode was found to be prompt, steady and reproducible during repeated on-off cycles of the visible light illumination. At low potentials, FTO/CdS revealed a cathodic photocurrent at -0.5 V (*ca*. -0.3 μA, 285 s), while FTO/*f*-MoS_2 appeared to be photoelectrochemically inactive (Figure 4b). For the FTO/MoS_2/CdS electrode, a small photocathodic response was observed at short times (-0.2 μA, 15 s). However, at longer times the presence of spikes masks the stationary photoelectrochemical response. Then, at high potentials (Figure 4c), excitation of the FTO/MoS_2/CdS electrode displayed an important anodic photocurrent value (+1.0 □A, 225 s), while the reference electrodes based on the individual species FTO/CdS and FTO/*f*-MoS_2 showed very low photoactivity (i.e. < 0.1 μA). The latter result confirms the strong interaction between CdS and MoS_2 within the MoS_2/CdS ensemble, further supports the existence of electron transfer from photoexcited CdS to MoS_2 and highlights the importance of excited-state interactions between CdS and MoS_2 for generating a photoelectrochemical effect. Although it cannot be completely ruled out, energy transfer in MoS_2/CdS would not yield a significant improvement of the photocurrent, since *f*-MoS_2 is not photoactive itself. Eventually, charge separation was evident by zero-current photopotential measurements as shown in Figure 4d. There, it can be seen that FTO/CdS reached a photopotential of +91 mV, which is in good agreement with a photocathodic and electron donor behavior, while FTO/*f*-MoS_2 gave a very small negative photopotential of -16 mV, which is consistent with a low photoactivity and an electron acceptor behavior. Notably, FTO/MoS_2/CdS gave a photopotential value of -540 mV, demonstrating strong charge-separation, where holes were easily transferred to the solution and electrons accumulate in MoS_2, thus yielding this high negative photopotential value.

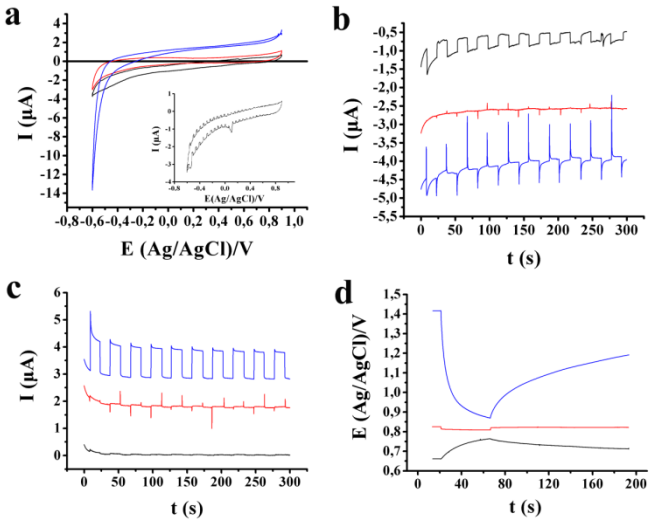

Figure 4. (a) Cyclic voltammograms under illumination. Inset image: on-off voltamogram for FTO/CdS. (b, c) photocurrents at -0.5 V and +0.8 V, respectively, and (d) photopotential at zero current, for FTO/MoS_2/CdS (blue), FTO/CdS (black) and FTO/*f*-MoS_2 (red). Photocurrents (in b and c) and photopotentials (in d) are offset for clarity. The spikes appearing in the photocurrent transients of *f*-MoS_2 are ascribed to recombination processes, which occur, at potentials slightly above (in absolute value) the onset potential, involving defects or trap sites.[38]

Conclusions

A facile protocol for the template synthesis of semiconducting CdS nanoparticles onto functionalized MoS_2 was developed. Specifically, functionalized MoS_2 with α-lipoic acid was employed for the in-situ growth of CdS. The CdS were preferentially immobilized at the carboxylate units of α-lipoic acid located at S-vacant sites in the periphery of MoS_2 nanosheets. The MoS_2/CdS ensemble was fully characterized by ATR-IR and Raman spectroscopy, while TGA allowed estimating the loading of CdS on MoS_2 and TEM imaging aided visualizing the morphology of CdS. Furthermore, strong electronic interactions at the excited state were identified to occur from the photoexcited CdS to MoS_2, evidenced by the efficient fluorescence emission quenching of CdS nanoparticles. Thin-film electrodes were fabricated by spray-coating of the MoS_2/CdS ensemble on FTO and the FTO/MoS_2/CdS electrode was evaluated as photoanode in photoelectrochemical cells. Prompt, steady and reproducible photoresponse was acquired for FTO/MoS_2/CdS during repeated on-off cycles of visible light illumination. Particularly, the enhanced photoactivity observed was rationalized by considering strong interactions and effective charge separation within the ensemble, where holes were easily transferred from CdS to the solution and electrons accumulate in MoS_2. Based on the results derived from the photoelectrochemical assays, we conclude that the fabrication of such nanoarchitectures constructed by MoS_2 and CdS, extendable not only to other TMDs but also to diverse quantum dots, may lead to the development of optoelectronic devices with improved characteristics.

Experimental Section

General

Chemicals, reagents, and solvents were purchased from Sigma-Aldrich and used as received. Infrared (IR) spectra were acquired on a Fourier Transform IR spectrometer (Equinox 55 from Bruker Optics) equipped with a single reflection diamond ATR accessory (DuraSamp1IR II by SensIR Technologies). Electronic absorption spectra (UV-Vis) were recorded on a PerkinElmer (Lambda 19) UV-Vis-NIR spectrophotometer. UV-Vis spectra of films were obtained in transmission mode using a Shimadzu UV-2401 PC spectrometer. Steady-state emission spectra were recorded on a Fluorolog-3 Jobin Yvon-Spex spectrofluorometer (model GL3-21). Thermogravimetric analysis was performed using a TGA Q500 V20.2 Build 27 instrument by TA in a nitrogen (purity >99.999%) inert atmosphere. TEM images were taken at room temperature using a JEOL JEM-2100F, operated at an acceleration voltage of 80 keV under a pressure of 10^{-5} Pa. The samples were sonicated in 3 mL hexane for 1 minute and 10 drops of the dispersion solution were deposited onto carbon-coated copper grids. TEM images were recorded on a Gatan MSC 794 1 k×1 k CCD camera with a typical exposure time of 0.3 s. Scanning electron microscopy (SEM) imaging and energy dispersive X-ray spectroscopy (EDX) were performed using a FE-SEM (model JSM-7610F) equipped with EDAX (X-ACT, Oxford instrument). The electrochemical characterization was performed with a AUTOLAB PGSTAT302N potentiostat. Cyclic voltammetry experiments were carried out in a three-electrode cell employing a 0.1 M $NaClO_4$ in dry acetonitrile as supporting electrolyte at a scan rate of 20 mV/s, using Ag/AgCl as a reference electrode. Photoelectrochemical measurements were carried out on spray-coated samples on FTO substrates (covering area 1 cm^2) as working electrode, which were illuminated through a quartz window by a 150 W Xenon arc lamp (LOT-Oriel GmbH, Germany). Electrodes were prepared by spraying identical amounts of mass of each material onto the FTO substrate.

Preparation of *f*-MoS_2

Exfoliated semiconducting MoS_2 nanosheets were prepared upon chlorosulfonic acid treatment of the bulk material.[31] Next, exfoliated MoS_2 (15 mg) and α-lipoic acid (10 mg) were dissolved in DMF (7 mL) and the reaction mixture was heated at 70 °C under stirring for three days. After that period, the reaction mixture was filtered over a PTFE membrane filter (pore size 0.2 μm) and the residue was extensively washed with dichloromethane to obtain *f*-MoS_2 as powder.

Preparation of MoS_2/CdS

Cadmium acetate (7 mg) dissolved in DMF (3 mL) was added to *f*-MoS_2 (4 mg) dissolved in DMF (20 mL), under vigorous stirring and the mixture was left under stirring overnight. Then, aqueous thioacetamide (2 mg in 500 μL) was added and the reaction mixture was heated at 80 °C for 15 minutes to afford MoS_2/CdS. The ensemble was purified by filtration over a PTFE membrane filter (pore size 0.2 μm) followed by extensive washing of the residue with dichloromethane.

Acknowledgements

This project has received funding from the European Union's Horizon 2020 research and innovation programme under the Marie Sklodowska-Curie grant agreement Nº 642742. Support of this work by the project "Advanced Materials and Devices" (MIS 5002409) which is implemented under the "Action for the Strategic Development on the Research and Technological Sector", which

is implemented under the “Reinforcement of the Research and Innovation Infrastructures”, funded by the Operational Program "Competitiveness, Entrepreneurship and Innovation" (NSRF 2014-2020) and co-financed by Greece and the European Union (European Regional Development Fund) is also acknowledged. A.M.B. and W.K.M. acknowledge Spanish MINEICO (project grant ENE2016-79282-C5-1-R, AEI/FEDER, UE) and the Gobierno de Aragón (Grupo Reconocido DGA T03_17R, FEDER, UE). We are indebted to the group of Prof. H. Shinohara, Nagoya University, Japan, for kindly helping with the TEM imaging.

Keywords: transition metal dichalcogenides, nanoparticles, hybrids, electron transfer, photoelectrochemical cell

[1] V. Strauss, A. Roth, M. Sekita, D.M Guldi, *Chem.* **2016**, *1*, 531-556.

[2] G. Bottari, M. A. Herranz, L. Wibmer, M. Volland, L. Rodriguez-Perez, D. M. Guldi, A. Hirsch, N. Martin, F. D’Souza, T. Torres, *Chem. Soc. Rev*. **2017**, *46*, 4464-4500.

[3] T. Umeyama, H. Imahori, *Nanoscale Horiz*. **2018**, *3*, 352-366.

[4] J. Cherusseri, N. Choudhary, K. S. Kumar, Y. Jung, J. Thomas, *Nanoscale Horiz*. **2019**, *4*, 840-858.

[5] R. Li, Y. Cheng*, Small* **2018**, *14*, 1802091.

[6] H. Wang, C. Li, P. Fang, Z. Zhang, J. Z. Zhang, *Chem. Soc. Rev.* **2018**, *47*, 6101-6127.

[7] M. Pumera, Z. Sofer, A. Ambrosia, *J. Mater. Chem*. A **2014**, *2*, 8981-8987.

[8] D. Voiry, J. Yang, M. Chhowalla*, Adv. Mater.* **2016**, *28*, 6197-6206.

[9] S. Rowley-Neale, C. Foster, G. Smith, D. Brownson, C. E. Banks, *Sustain. Ener. Fuels* **2017**, *1*, 74-83.

[10] D. K. Perivoliotis, N. Tagmatarchis, *Carbon* **2017**, *118*, 493-510.

[11] A. Kagkoura, T. Skaltsas, N. Tagmatarchis, *Chem. Eur. J.* **2017**, *23*, 12967-12979.

[12] A. Stergiou, N. Tagmatarchis, *Chem. Eur. J.* **2018**, *24*, 18246-18257.

[13] R. Canton-Vitoria, Y. Sayed-Ahmad-Baraza, M. Pelaez-Fernandez, R. Arenal, C. Bittencourt, C. P. Ewels, N. Tagmatarchis, *npj 2D Mater. Appl.* **2017**,*1*,13.

[14] R. Canton-Vitoria, H. B. Gobeze, V. M. Blas-Ferrando, J. Ortiz, Y. Jang, F. Fernández-Lázaro, A. Sastre-Santos, Y. Nakanishi, H. Shinohara, F. D'Souza, N. Tagmatarchis, *Angew. Chem. Int. Ed.* **2019**, *58*, 5712-5717.

[15] L. Vallan, R. Canton-Vitoria, H. B. Gobeze, Y. Jang, R. Arenal, A. M. Benito, K.M. Maser, F. D’Souza, N. Tagmatarchis, *J. Am. Chem. Soc.* **2018**, *140*,13488-13496.

[16] R. Canton-Vitoria, C. Stangel. N. Tagmatarchis, *ACS Appl. Mater. Interfaces* **2018**, *10*, 23476-23480.

[17] R. Canton-Vitoria, L. Vallan, E. Urriolabeitia, A. M. Benito, W. K. Maser, N. Tagmatarchis, *Chem. Eur. J.* **2018**, *24*, 10468-10474.

[18] S. Kundu, A. Patra, *Chem. Rev.* **2017**, *117*, 712-757.

[19] R. S. Selinsky, Q. Ding, M. S. Faber, J. C. Wright, S. Jin, *Chem. Soc. Rev.* **2013**, *42*, 2963-2985.

[20] G. H. Carey, A. L. Abdelhady, Z. Ning, S. M. Thon, O. M. Bakr, E. H. Sargent, *Chem. Rev.* **2015**, *115*, 12732-12763.

[21] M. G. Walter, E. L. Warren, J. R. McKone, S. W. Boettcher, Q. Mi, E. A. Santori, N. S. Lewis, *Chem. Rev.* **2010**, *110*, 6446-6473.

[22] G. Mountrichas, A. S. D. Sandanayaka, S. P. Economopoulos, S. Pispas, O. Ito, T. Hasobe, N. Tagmatarchis, *J. Mater. Chem.* **2009**, *19*, 8990-8998.

[23] Y. Liu, Y. Yu, W. Zhang, *J. Phys. Chem. C* **2013**, *117*, 12949-12957.

[24] Z. Yan, L. Du, D. L. Phillips, *RSC Adv.* **2017**, *7*, 55993-55999.

[25] B. Han, S. Liu, N. Zhang, Y. Xu, T. Tang, *Appl. Catal. B* **2017**, *202*, 298-304.

[26] X. Zong, H. J. Yan, G. P. Wu, G. J. Ma, F. Y. Wen, L. Wang, C. Li*, J. Am. Chem. Soc.* **2008**, *130*, 7176-7177.

[27] X. Zong, G. P. Wu, H. J. Yan, G. J. Ma, J. Y. Shi, F. Y. Wen, L. Wang, C. Li, *J. Phys. Chem. C* **2010**, *114*, 1963-1968.

[28] W, Gu, F. Yang, C. Wu, Y. Zhang, M. Shi, X. Ma, *Nanoscale Res. Lett.* **2014**, *9*, 662.

[29] G. Mountrichas, S. Pispas, N. Tagmatarchis, *Small* **2007**, *3*, 404-407.

[30] R. Canton-Vitoria, E. Istif, J. Hernández-Ferrer, E. Urriolabeitía, A. M. Benito, W. K. Maser N. Tagmatarchis, *ACS Appl. Mater. Interfaces* **2019**, *11*, 5947-5956. [31] G. Pagona, C. Bittencourt, R. Arenal, N. Tagmatarchis, *Chem. Commun.* **2015***, 51*, 12950-12953.

[32] A. P. Nayak, T. Pandey, D. Voiry, J. Liu, S. T. Moran, A. Sharma, C. Tan, C-H. Chen, L.-J. Li, M, Chhowalla, J.-F. Lin, A. K. Singh, D. Akinwande, *Nano Lett.* **2015**, *15*, 346-353.

[33] G. C. Papavasiliou, *Prog. Solid State Chem.* **1997**, *25*, 125-170.

[34] Y. Song, H. Hu, M. Feng, H. Zhan, *ACS Appl. Mater. Interfaces* **2015**, *7*, 25793-25803.

[35] X. Chen, L. Liu, F. Huang*, Chem. Soc. Rev.* **2015**, *44*, 1861-1885.

[36] E. Istif, J. Hernandez-Ferrer, E. P. Urriolabeitia, A. Stergiou, N. Tagmatarchis, G. Fratta, M. J. Large, A. B. Dalton, A. M. Benito, W. K. Maser, *Adv. Funct. Mater.* **2018**, *28*, 1707548.

[37] S. Pan, H. Rao, I. Mora-Sero, J. Bisquert, X. Zhong, *Chem. Soc. Rev.* **2018**, *47*, 7659-7702.

[38] T. Berger, D. Monllor-Satoca, M. Jankulovska, T. Lana-Villarreal, R. Gómez, *ChemPhysChem* **2012**,*13*, 2824-2875.

Entry for the Table of Contents

In-situ growth of CdS nanoparticles on functionalized MoS_2 showing enhanced photoactivity